SI Appendix

Materials and Methods

Cell culture. U-251, LN-18 and U-87 glioblastoma cells were purchased from ATCC and cultured in DMEM H-21 medium containing 5% FBS. All cells contained 1X penicillin/streptomycin in their respective media (Thermo Fisher Scientific) and were passaged every 2-3 days (37ºC and 5% CO_2). For *in vivo* experiments, the U-251 cells were cultured up to the time of subcutaneous or intracranial injection when they were resuspended in DMEM medium alone. For the EGF stimulation experiment, U-251 and LN-18 cells were starved for 24h before the addition of H_2O (vehicle) or EGF only (100ng/ml; PeproTech) for 24h. The 3832 human glioblastoma stem-like neurosphere line (a gift from Dr. Jeremy Rich from the School of Medicine at the University of California San Diego, San Diego, CA) and the 218 low-passage glioblastoma cells were grown in neurobasal medium containing supplements (1X N2 supplement and 1X Glutamax from Thermo Fisher Scientific) and FGF and EGF (25ng/ml from PeproTech). All cell lines were confirmed mycoplasma negative using MycoFluor™ Mycoplasma Detection Kit (Thermo Fisher Scientific).

Quantitative real-time polymerase chain reaction (qRT-PCR) analysis. Gene expression was assessed as previously reported (1).

Transfections and generation of stable transformants. *Control pcDNA3 and TLN1 plasmids* were transfected as previously described (1). All cells were generated by infection with a lentivirus containing anti-luc or anti-*PHIP* shRNA as previously described (1).

Colony formation assay. This assay was carried out as previously described (1).

Cell viability. 3832 primary, patient-derived glioblastoma cells were plated in 96-well plates at a density of 10,000 cells per well in triplicates. Cell viability was assessed at 14 days using Cell Counting Kit-8 (Dojindo Molecular Technologies) following the manufacturer's instructions.

Cell cycle analysis. This analysis was performed as previously described (2).

Migration assays. *Wound assay:* Cells were grown to confluency on 10cm petri dishes and a scratch was introduced by using a pipette tip. Medium was immediately replaced to remove floating cells. Adherent cells were grown for 2 days when pictures were taken.

Boyden chamber assay: Anti-*PHIP* shRNA-expressing U-251 and LN-18 cells were infected with *GFP-Zyxin* cDNA fusion lentiviral particles (GeneTarget Inc; LVP449-G) before the migration assay in transwells. 5,000 cells (U-251 or LN-18 stable transformants) were seeded in the transwell without serum and allowed to migrate to the lower chamber filled with culture medium containing 10% FBS. After overnight migration, the cells were fixed with 2.5% glutaraldehyde, stained with toluidine blue and counted under the microscope (n=6 for every stable transformant).

Invasion assay. The Matrigel assay for tumor invasion was performed as described (1). U-251 and LN-18 cells were starved for 4h before plating them on the transwells. Insert chambers were coated with 15 µl Matrigel at 7mg/ml protein for U-251 and U-87 cells, 5mg/ml protein for LN-18 cells and 3mg/ml protein for 3832 and 218 cells.

Tissue arrays and immunostaining. A glioma tissue array was purchased from US Biomax Inc. Samples were stained with anti-human PHIP monoclonal antibody at a 1:100 dilution (Abnova, H00055023-M01). Microwave antigen retrieval was conducted

in 10mM citrate buffer, pH 6.0. Endogenous peroxidase was blocked with 3% H_2O_2, and additional blocking was performed with normal rabbit serum. The primary antibody was diluted in 1.0% BSA in PBS and applied overnight at 4°C. Antibody staining was observed by using a one-step polymer-HRP IHC detection system (Biogenex; QD600-60K). The regions of most uniform staining were scored for each specimen and the expression of PHIP protein was graded on cellular intensity using the following scale: no staining (0), weak staining (1), moderate staining (2), and intense staining (3). The tissue microarrays and positive and negative control sections were scored (by L. Soroceanu) twice, and a third, consensus score was determined for any discrepant scoring. Microvessel density analysis was performed by staining mouse brain sections with a rabbit CD31 antibody (Abcam; ab28364 at 1:1000 dil.), followed by one-step polymer-HRP IHC detection system (Biogenex). Fourteen fields totaling 8mm^2 were analyzed at 40x magnification with a Mirax Midi Digital Platform (Zeiss). The number of CD31-positive vessels was quantitated using ImageJ software (NIH, Bethesda, MD), and the microvessel density reported as the average of CD31 counts for three Luc shRNA samples *versus* three *PHIP* shRNA samples.

Western analysis. U-251 and LN-18 stable transformants were starved for 3 days in DMEM medium only before protein extraction that was carried out from adherent cells according to the manufacturer's protocol (Santa Cruz Biotechnology). 50µg of protein was electrophoresed and detected as previously described (1). The following antibodies were utilized: PHIP (Abnova; H00055023-M01 at 1:500 dil.), pAKT (Ser473) (Cell Signaling; 9271 at 1:1000 dil.), total AKT (Cell Signaling; 9272 at 1:2000 dil.), GAPDH (EMD Millipore; MAB374 at 1:1000 dil.), pPXN (Tyr118) (Cell Signaling; 2541 at 1:1000

dil.), cyclin D1 (CCND1) (Santa Cruz Biotechnology; sc-718 at 1:1000 dil.), VCL (Bethyl Laboratories; A302-535A at 1:4000), goat anti-mouse HRP (EMD Millipore; 12-349 at 1:1000 dil.), and bovine anti-rabbit HRP (Santa Cruz Biotechnology; sc-2370 at 1:1000 dil.).

Human phospho-kinase profiling. We analyzed the phosphorylation profiles of kinases and their protein substrates using a proteome profiler array (R&D Systems; ARY003) on U-251 stable transformants expressing either an anti-luc shRNA or an anti-*PHIP* shRNA#1 following the manufacturer's protocol.

Fluorescence microscopy. Fluorescence imaging of PHIP was performed on cells cultured on coverslips as previously described (1). The quantitative analysis of immunopositivity of the target proteins was carried out either using AxioVision software (Zeiss) or ImageJ using a plugin for generating a profile of pixel intensity at the leading edge of the cells.

The following primary antibodies were used: PHIP (Abnova; H00055023-M01 at 1:250 dil.); VCL (Sigma; V4505 at 1:500 dil.); ITGB1 (Santa Cruz Biotechnology; sc-8978 at 1:250 dil.); pPXN (Y118) (Cell signaling; 2541 at 1:500 dil.); pFAK (Y925) (Cell signaling; 3284 at 1:250 dil.); TLN1 (Abcam; ab71333 at 1:500 dil.); ZYX (Abcam; ab50391 at 1:500 dil.); and Rhodamine-phalloidin (Thermo Fisher Scientific; R415 at 1:40 dil.). All cells were plated on coverslips previously coated with 10μg/ml laminin (Sigma; L2020-1mg).

FISH analysis. FISH for *PHIP* copy number was performed as previously described (3) using bacterial artificial chromosome (BAC) clones RP11-767O1 and CTD-2297E14 to detect the PHIP locus and clones RP11-26M18 and RP11-136K2 to detect 6q11.1 and

6p11.1, respectively (interpreted as chromosome 6 centromere). FISH for *EGFR* copy number was performed using BAC clone RP11-81B20. For a chromosome 7-specific probe, BAC clone RP11-45N18 was used to detect 7q11.21 (all BAC clones were obtained from the Children's Hospital Oakland Research Institute). The quality and mapping of all probes were verified by hybridization to normal metaphase spreads in combination with a commercially available centromeric probe for chromosomes 6 and 7 (Empire Genomics LLC, New York) before tissue analysis. Z-stacked images were acquired using a Zeiss Axio Image Z2 microscope controlled by AxioVision software (Zeiss). At least 50 nuclei from each case were evaluated, and the signals were interpreted according to guidelines described previously (4). Signals from BAC clones detecting 6q11.1, 6p11.1, and 7q11.21 were interpreted as the centromeric signal for chromosome 6 and 7, respectively.

VEGF ELISA. VEGF secretion in U-251 stable transformants was detected using the Human VEGF Duo set (R&D Systems**;** DY293B**)** according to the manufacturer's instructions.

Time-lapse and confocal microscopy. Cells were plated at 20,000–40,000 cells/well in 6-well culture plates. Cultures were transferred from the incubator to a time-lapse microscope, controlled by Zen 2 Imaging software (Zeiss) equipped with a heated stage and a Plexiglass environmental chamber (Axiovert 200; Zeiss) that maintained optimum cell culture environment. Phase contrast and fluorescent images from each well were taken in 300 s intervals with a Hamamatsu ORCA-ER (Hamamatsu Photonics, Japan) CCD camera. Rendering of movies was performed using Zen 2 software (Zeiss). Cell tracking and motility measurements were performed using ImageJ and MTrackJ plugin.

Confocal imaging was performed using a Zeiss LSM 880 with Airyscan detector. The system was controlled using Zeiss Zen 2 software and images were analyzed using Imaris software (Bitplane AG).

Cytoplasmic and nuclear fractionation. U-251 cells were stimulated with 5µg/ml of insulin for 30min before nuclear and cytoplasmic fractionation as previously described (1).

Coimmunoprecipitation. 1mg of cytoplasmic protein extract was incubated overnight with anti-human PHIP (Bethyl Laboratories; A302-055A at 1µg), anti-human VCL (Sigma; V4505 at 1µg) or anti-rabbit IgG control (Santa Cruz Biotechnology; sc-2028 at 1µg) antibodies as previously described (1).

Quantitative real-time polymerase chain reaction (qRT-PCR) analysis and glioblastoma subtyping. Gene expression was assessed as previously reported (1). mRNAs were assayed using the TaqMan Gene Expression Assays in accordance with the manufacturer's instructions (Thermo Fisher Scientific). TaqMan probes for *PHIP* (Hs00215670_m1), *VCL* (Hs00419715_m1), *PXN* (Hs01104424_m1) and *TLN1* (Hs00559595_m1) were purchased from Thermo Fisher Scientific. The expression levels of these genes were normalized to either the human *HPRT1* (Hs02800695_m1) or *RAB14* (Hs00249440_m1) genes before comparisons.

Glioblastoma subtyping. Our cohort of 25 fresh frozen cases were subtyped by using RNAseq and/or by TaqMan assays with a specific panel of 15 genes (5 for every subtype) previously described (5). The following TaqMan probes were used to classify glioblastoma cases and gene expression was normalized to the human *RAB14* gene (Hs00249440_m1) before comparisons:

Mesenchymal: TNFRS1 (Hs0104232_m1), *RELB* (Hs00232399_m1), *CHI3L1* (Hs01072228_m1), *CEBPB* (Hs00270923_s1), *CD44* (Hs01075861_m1).

Classical: TIMP3 (Hs00165949_m1), *NOTCH3* (Hs00166432_m1), *NES* (Hs00707120_s1), *EGFR* (Hs01076078_m1), *AKT2* (Hs01086102_m1).

Proneural: SOX11 (Hs00846583_s1), *SOX2* (Hs01053049_s1), *PDGFRA* (Hs00998018_m1), *OLIG2* (Hs00377820_m1), *BCAN* (Hs00222607_m1).

RNA-Seq: RNA was extracted from frozen tumor samples by using the RNAeasy mini kit (Qiagen). RNA-Seq was performed from ~500ng of total RNA processed using TruSeq polyA selection, at a target depth of 40 million paired-end, stranded reads on an Illumina 2500. For RNA-Seq analysis, gene expression values were obtained using the Kallisto algorithm in AltAnalyze (6) version 2.1.1. Differential gene expression was performed using an empirical Bayes moderated t-test, following FDR correction ($p<0.05$). Additional gene set enrichment, hierarchical clustering and data visualizations were generated using AltAnalyze (6-9).

Animal studies. All animal care was in accordance with institutional guidelines and a protocol that was approved by the CPMC Research Institute on Animal Care and Use Committee. Groups of 5 45-day-old female nude mice (Harlan laboratories) were inoculated by subcutaneous injection with $2x10^6$ U-251 stable transformants in medium containing 50% Matrigel or groups of 8 mice with 350,000 cells in plain medium for intracranial injection. Subcutaneous tumor volume was measured using the formula: Volume = (Length x $Width^2$)/2. The area of intracranial tumors was measured using Mirax Midi Digital Platform (Zeiss).

Statistical methods. All quantified data represents an average of at least triplicate samples or as indicated. Error bars represent standard deviation of the mean. Statistical significance was determined by the Student's *t*-test, Mann-Whitney test, ANOVA, or Kolmogorov-Smirnov (K-S) test, and p values <0.05 were considered significant.

Supplementary Figures and Videos

Fig. S1. Effects of stable suppression of *PHIP* in U-251 cells *in vitro*. (*A*) Relative expression of the *PHIP* gene in U-251 transformants stably expressing an anti-luc shRNA or anti-*PHIP* shRNA#1 (*B*) Western analysis of PHIP and other proteins in U-251 transformants stably expressing an anti-luc shRNA or anti-*PHIP* shRNA#1. (*C*) Phosphorylation profiles of kinases and their protein substrates in U-251 transformants stably expressing an anti-luc shRNA or anti-*PHIP* shRNA#1. (*D*) Relative expression of *PHIP* in U-251 transformants stably expressing an anti-luc shRNA or anti-*PHIP* shRNA#2. (*E*) Quantitative immunofluorescence of PHIP at the leading edge of U-251 transformants stably expressing an anti-luc shRNA or anti-*PHIP* shRNA#2. (*F*) Phase contrast images of scratch assay at 0h and 24h post-wound and quantification of the area covered by U-251 transformants stably expressing an anti-luc shRNA or anti-*PHIP* shRNA#2. (*G*) Invasion assay of U-251 transformants stably expressing an anti-luc shRNA or anti-*PHIP* shRNA#2, with representative images. (*H*) Colony formation ability of U-251 transformants stably expressing an anti-luc shRNA or anti-*PHIP* shRNA#2, with representative images. All graphs represent mean±s.e.m. *denotes $p<0.05$ *versus* control.

Fig. S2. Qualitative immunofluorescence analysis of PHIP and focal adhesion proteins in U-251 cells stably expressing an anti-luc shRNA or anti-*PHIP* shRNA#1. Images representing immunofluorescent detection of (*A*) PHIP and pFAK (Y925), (*B*) PHIP and ITGB1 in U-251 transformants. DAPI staining was used to counterstain the nuclei (scale bar indicates 20 μm). White arrows point to the leading edge of cells. Quantification of the immunofluorescence results, including statistical analysis, is provided in Fig. S3.

Fig. S3. Quantitative immunofluorescence of proteins at the leading edge of U-251 stable cells. (*A*) PHIP, (*B*) ITGB1, (*C*) pPXN (Y118), (*D*) pFAK (Y925), (*E*) VCL, (*F*) ZYX, (*G*) F-actin in U-251 transformants stably expressing an anti-luc shRNA or anti-*PHIP* shRNA#1. Statistical analysis of differences in protein expression was performed using the K-S test.

Fig. S4. Qualitative immunofluorescence analysis of PHIP and focal adhesion proteins in LN-18 transformants stably expressing an anti-luc shRNA or anti-*PHIP* shRNA#1. Images representing immunofluorescent detection of PHIP and pFAK (Y925), PHIP and pPXN and PHIP and ITGB1 in LN-18 transformants. DAPI staining was used to counterstain the nuclei (scale bar indicates 20 μm). White arrows point to the leading edge of cells. Quantification of the immunofluorescence results, including statistical analysis, is provided in Fig. S6.

Fig. S5. Qualitative immunofluorescence analysis of PHIP and focal adhesion proteins in LN-18 cells. Images representing immunofluorescent detection of (*A*) TLN1, (*B*) ZYX and (*C*) VCL (upper panel) and F-actin (lower panel) in LN-18 transformants stably expressing an anti-luc shRNA or anti-*PHIP* shRNA#1. DAPI staining was used to counterstain the nuclei (scale bar indicates 20 μm). White arrows point to the leading edge of cells. (*D*) Representative confocal images (single Z-stack) of LN-18 cells after performing immunostaining for PHIP, TLN1 and VCL. DAPI staining was used to counterstain the nuclei (scale bar indicates 20 μm). (*E*) Graph showing percentage of area that PHIP colocalizes with the covisualized proteins in consecutive Z-stacks. Quantification of the immunofluorescence results, including statistical analysis, are provided in Fig. S6.

Fig. S6. Quantitative immunofluorescence of proteins at the leading edge of LN-18 stable cells. (*A*) PHIP, (*B*) ITGB1, (*C*) pPXN (Y118), (*D*) pFAK (Y925), (*E*) VCL, (*F*) ZYX, (*G*) F-actin in LN-18 transformants stably expressing an anti-luc shRNA or anti-*PHIP* shRNA#1. Statistical analysis of differences in protein expression was performed using the K-S test.

Fig. S7. Effects of stable suppression of *PHIP* in LN-18 and U-87 cells *in vitro*. (*A*) Relative expression of the *PHIP* gene in LN-18 transformants stably expressing an anti-luc shRNA or anti-*PHIP* shRNA#2. (*B*) Quantitative immunofluorescence of PHIP expression at the leading edge of LN-18 transformants stably expressing an anti-luc shRNA or anti-*PHIP* shRNA#2. (*C*) Phase contrast images of scratch assay at 0h and 24h post-wound, and quantification of the area covered by LN-18 transformants stably expressing anti-luc shRNA or anti-*PHIP* shRNA#2. (*D*) Invasion into Matrigel of LN-18 transformants stably expressing an anti-luc shRNA or anti-*PHIP* shRNA#2. (*E*) Colony formation ability of LN-18 transformants stably expressing an anti-luc shRNA or anti-*PHIP* shRNA#2. (*F*) Relative expression of the *PHIP* gene in U-87 transformants stably expressing anti-luc shRNA or anti-*PHIP* shRNA#1. (*G*) Qualitative immunofluorescence of PHIP expression in U-87 transformants stably expressing anti-luc shRNA or anti-*PHIP* shRNA#1 (scale bar indicates 20 μm). (*H*) Quantitative immunofluorescence of PHIP expression in U-87 transformants stably expressing anti-luc shRNA or anti-*PHIP* shRNA#1. Statistical analysis of differences in protein expression was performed using the K-S test. (*I)* Western analysis of pAKT and other proteins in U-87 transformants stably expressing anti-luc shRNA or anti-*PHIP* shRNA#1. (*J*) Invasion into Matrigel of U-87 transformants stably expressing anti-luc shRNA or anti-*PHIP* shRNA#1. (*K*) Colony

formation ability of U-87 transformants stably expressing anti-luc shRNA or anti-*PHIP* shRNA#1. (*L*) Quantitative immunofluorescence of PHIP expression in U-87 transformants stably expressing anti-luc shRNA or anti-*PHIP* shRNA#2. (*M*) Invasion into Matrigel of U-87 transformants stably expressing anti-luc shRNA or anti-*PHIP* shRNA#2. (*N*) Colony formation ability of U-87 transformants stably expressing anti-luc shRNA or anti-*PHIP* shRNA#2. All graphs represent mean±s.e.m. *denotes $p<0.05$ *versus* control.

Fig. S8. Effects of modulation of PHIP expression in glioblastoma cells. Quantitative immunofluorescence analysis of expression of (*A*) PHIP, (*B*) TLN1, and (*C*) ZYX in 3832 transformants stably expressing anti-luc shRNA or anti-*PHIP* shRNA#1. Statistical analysis of differences in protein expression was performed using the K-S test. (*D*) Quantitative immunofluorescence of PHIP expression in U-251 cells upon EGF stimulation. (*E*) Qualitative immunofluorescence of PHIP in LN-18 cells upon stimulation with EGF *versus* vehicle (scale bar indicates 20 μm). (*F*) Quantitative immunofluorescence of PHIP expression in LN-18 cells upon EGF stimulation. Statistical analysis of differences in protein expression was performed using the K-S test. All graphs represent mean±s.e.m. *denotes $p<0.05$ *versus* control. Quantitative immunofluorescence analysis of expression of (*G*) PHIP and (*H*) TLN1 in primary 218 cells stably expressing anti-luc shRNA or anti-*PHIP* shRNA#1. Statistical analysis of differences in protein expression was performed using the K-S test. (*I*) Qualitative immunofluorescence of ZYX expression in primary 218 cells following expression of anti-*PHIP* shRNA#1 *versus* anti-luc shRNA (scale bar indicates 20 μm). White arrows point to the leading edge of cells. (*J*) Quantitative immunofluorescence analysis of

expression of ZYX in primary 218 cells stably expressing anti-luc shRNA or anti-*PHIP* shRNA#1. Statistical analysis of differences in protein expression was performed using the K-S test. (*K*) Invasion into Matrigel of primary 218 cells expressing anti-*PHIP* shRNA or anti-luc shRNA.

Video S1: Qualitative analysis of migrating luc shRNA-expressing U-251 cells (scale bar indicates 50 μm).

Video S2: Qualitative analysis of migrating *PHIP* shRNA-expressing U-251 cells (scale bar indicates 50 μm).

Video S3: Qualitative analysis of GFP-tagged ZYX localization dynamics in luc shRNA-expressing U-251 cells (scale bar indicates 20 μm).

Video S4: Qualitative analysis of GFP-tagged ZYX localization dynamics in *PHIP* shRNA-expressing U-251 cells (scale bar indicates 20 μm).

Video S5: Qualitative analysis of GFP-tagged ZYX localization dynamics in luc shRNA-expressing LN-18 cells (scale bar indicates 20 μm).

Video S6: Qualitative analysis of GFP-tagged ZYX localization dynamics in *PHIP* shRNA-expressing LN-18 cells (scale bar indicates 20 μm).

Video S7: Qualitative analysis of migrating luc shRNA-expressing 3832 cells (scale bar indicates 50 μm).

Video S8: Qualitative analysis of migrating *PHIP* shRNA-expressing 3832 cells (scale bar indicates 50 μm).

References

1. de Semir D*, et al.* (2018) PHIP as a therapeutic target for driver-negative subtypes of melanoma, breast, and lung cancer. *Proc Natl Acad Sci U S A*.

2. Dar AA*, et al.* (2008) Frequent overexpression of Aurora Kinase A in upper gastrointestinal adenocarcinomas correlates with potent antiapoptotic functions. *Cancer* 112(8):1688-1698.
3. Bezrookove V*, et al.* (2018) Role of Elevated PHIP Copy Number as a Prognostic and Progression Marker for Cutaneous Melanoma. *Clin Cancer Res* 24(17):4119-4125.
4. Bayani J & Squire J (2004) Multi-color FISH techniques. *Curr Protoc Cell Biol* Chapter 22:Unit 22 25.
5. Verhaak RG*, et al.* (2010) Integrated genomic analysis identifies clinically relevant subtypes of glioblastoma characterized by abnormalities in PDGFRA, IDH1, EGFR, and NF1. *Cancer Cell* 17(1):98-110.
6. Emig D*, et al.* (2010) AltAnalyze and DomainGraph: analyzing and visualizing exon expression data. *Nucleic Acids Res* 38(Web Server issue):W755-762.
7. Salomonis N*, et al.* (2010) Alternative splicing regulates mouse embryonic stem cell pluripotency and differentiation. *Proc Natl Acad Sci U S A* 107(23):10514-10519.
8. Soroceanu L*, et al.* (2013) Id-1 is a key transcriptional regulator of glioblastoma aggressiveness and a novel therapeutic target. *Cancer Res* 73(5):1559-1569.
9. Olsson A*, et al.* (2016) Single-cell analysis of mixed-lineage states leading to a binary cell fate choice. *Nature* 537(7622):698-702.

Figure S1

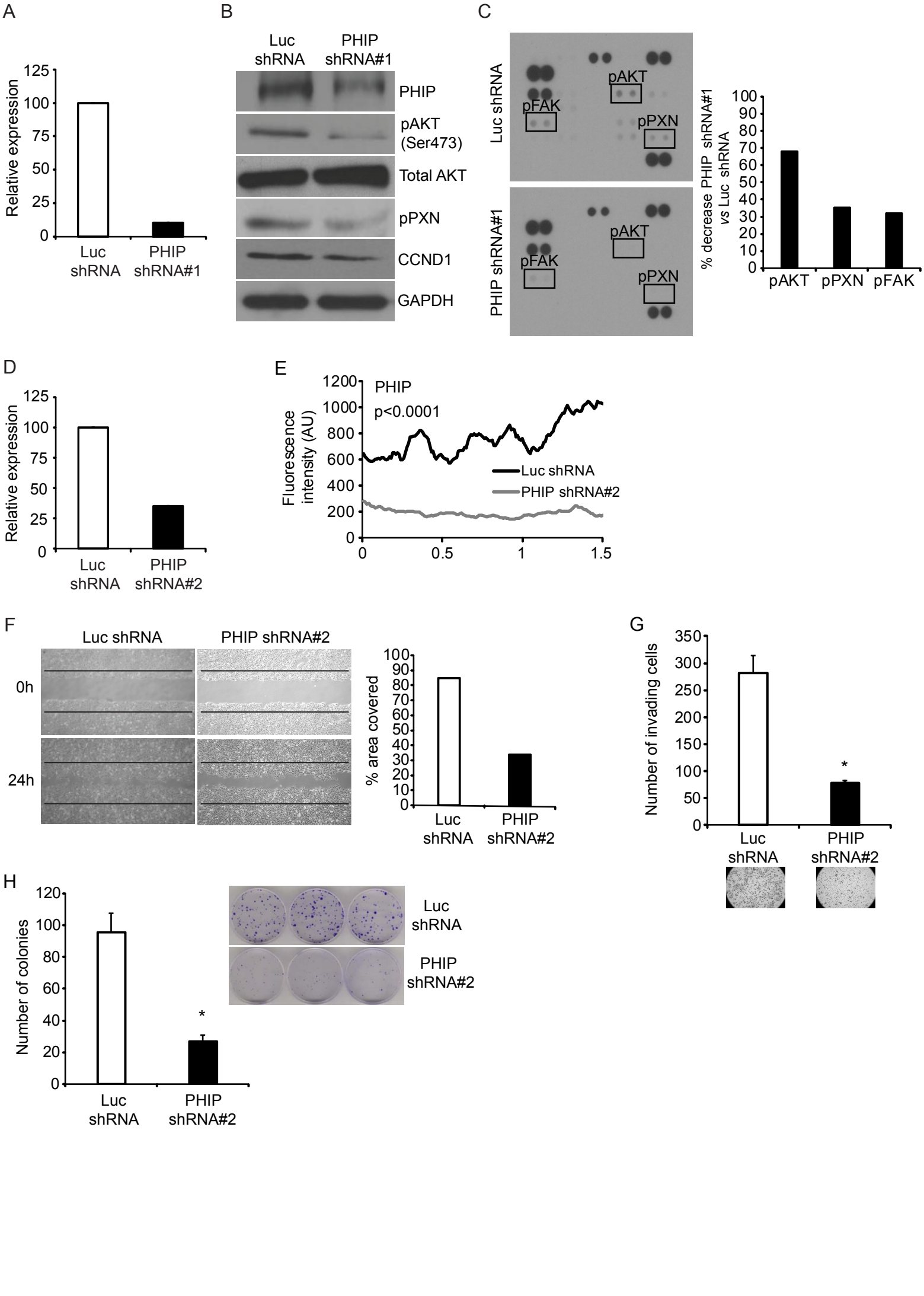
A
Relative expression
125
100
75
50
25
0
Luc shRNA
PHIP shRNA#1
B
Luc shRNA
PHIP shRNA#1
PHIP
pAKT (Ser473)
Total AKT
pPXN
CCND1
GAPDH
C
Luc shRNA
PHIP shRNA#1
pAKT
pFAK
pPXN
% decrease PHIP shRNA#1 vs Luc shRNA
100
90
80
70
60
50
40
30
20
10
0
pAKT
pPXN
pFAK
D
Relative expression
125
100
75
50
25
0
Luc shRNA
PHIP shRNA#2
E
PHIP
p<0.0001
Fluorescence intensity (AU)
1200
1000
800
600
400
200
0
0
0.5
1
1.5
Luc shRNA
PHIP shRNA#2
F
Luc shRNA
PHIP shRNA#2
0h
24h
% area covered
100
90
80
70
60
50
40
30
20
10
0
Luc shRNA
PHIP shRNA#2
G
Number of invading cells
350
300
250
200
150
100
50
0
*
Luc shRNA
PHIP shRNA#2
H
Number of colonies
120
100
80
60
40
20
0
*
Luc shRNA
PHIP shRNA#2
Luc shRNA
PHIP shRNA#2

Figure S2

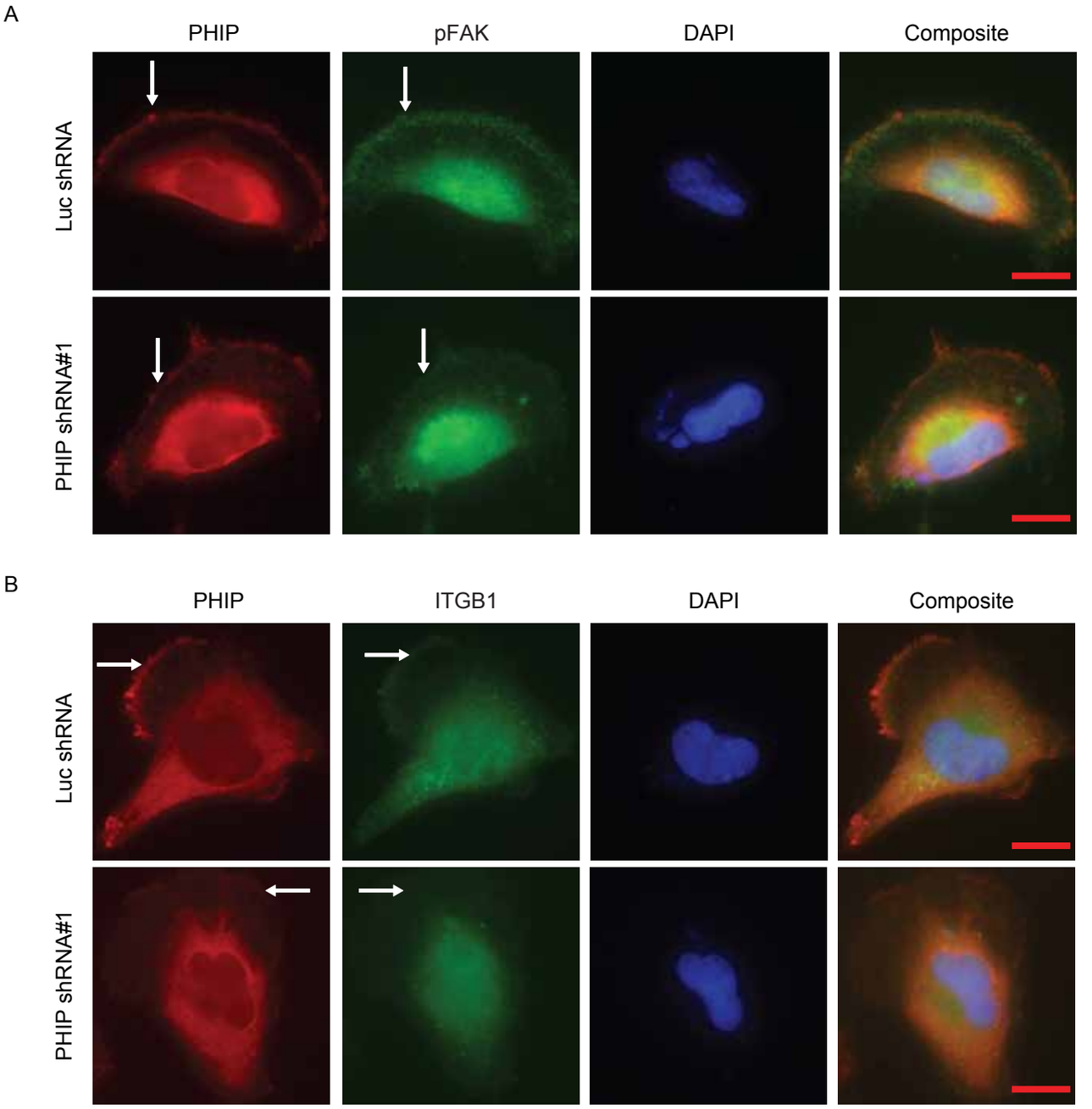
A
PHIP
pFAK
DAPI
Composite
Luc shRNA
PHIP shRNA#1
B
PHIP
ITGB1
DAPI
Composite
Luc shRNA
PHIP shRNA#1

Figure S3

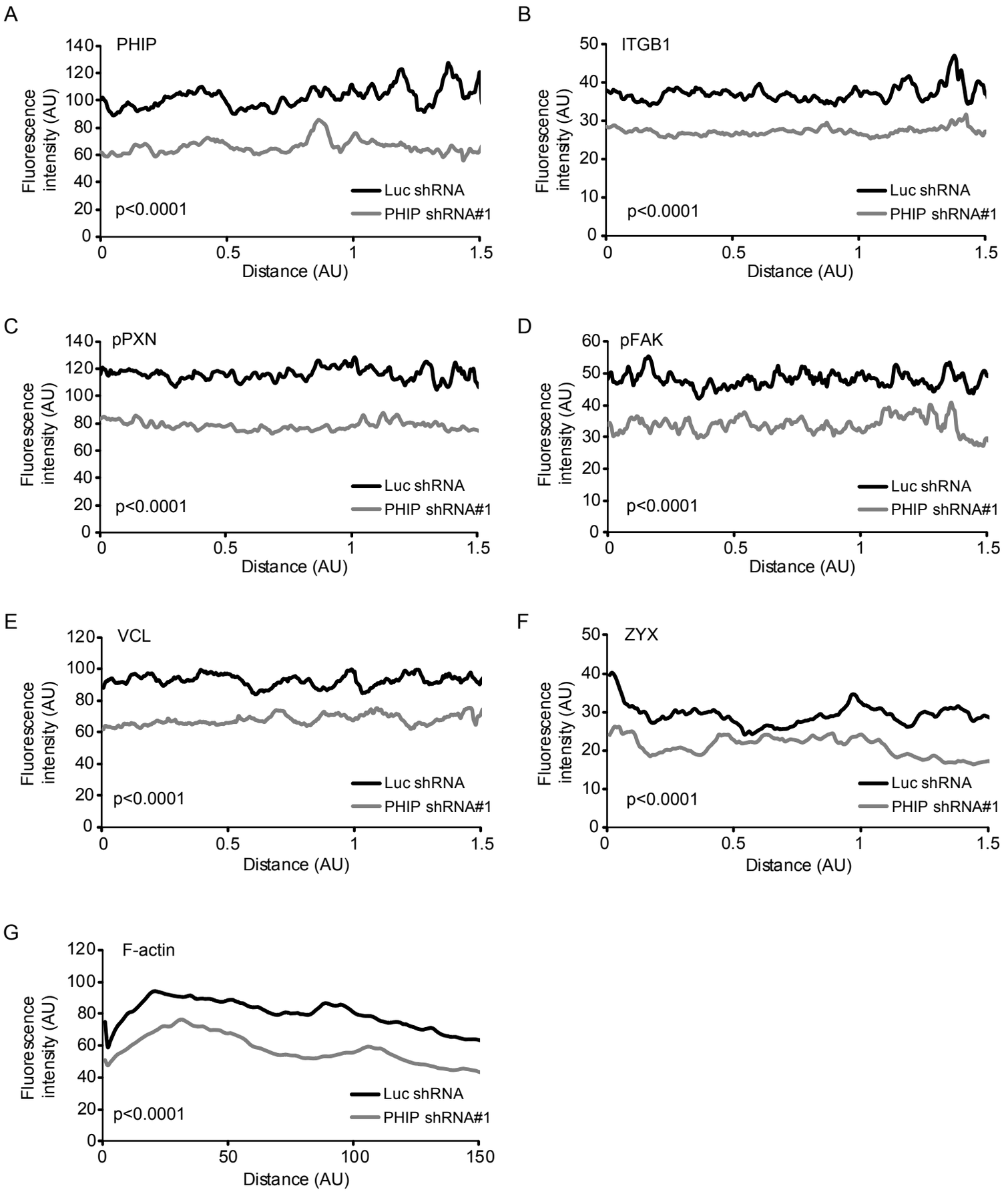
A
PHIP
Fluorescence intensity (AU)
Distance (AU)
Luc shRNA
PHIP shRNA#1
p<0.0001
B
ITGB1
C
pPXN
D
pFAK
E
VCL
F
ZYX
G
F-actin

Figure S4

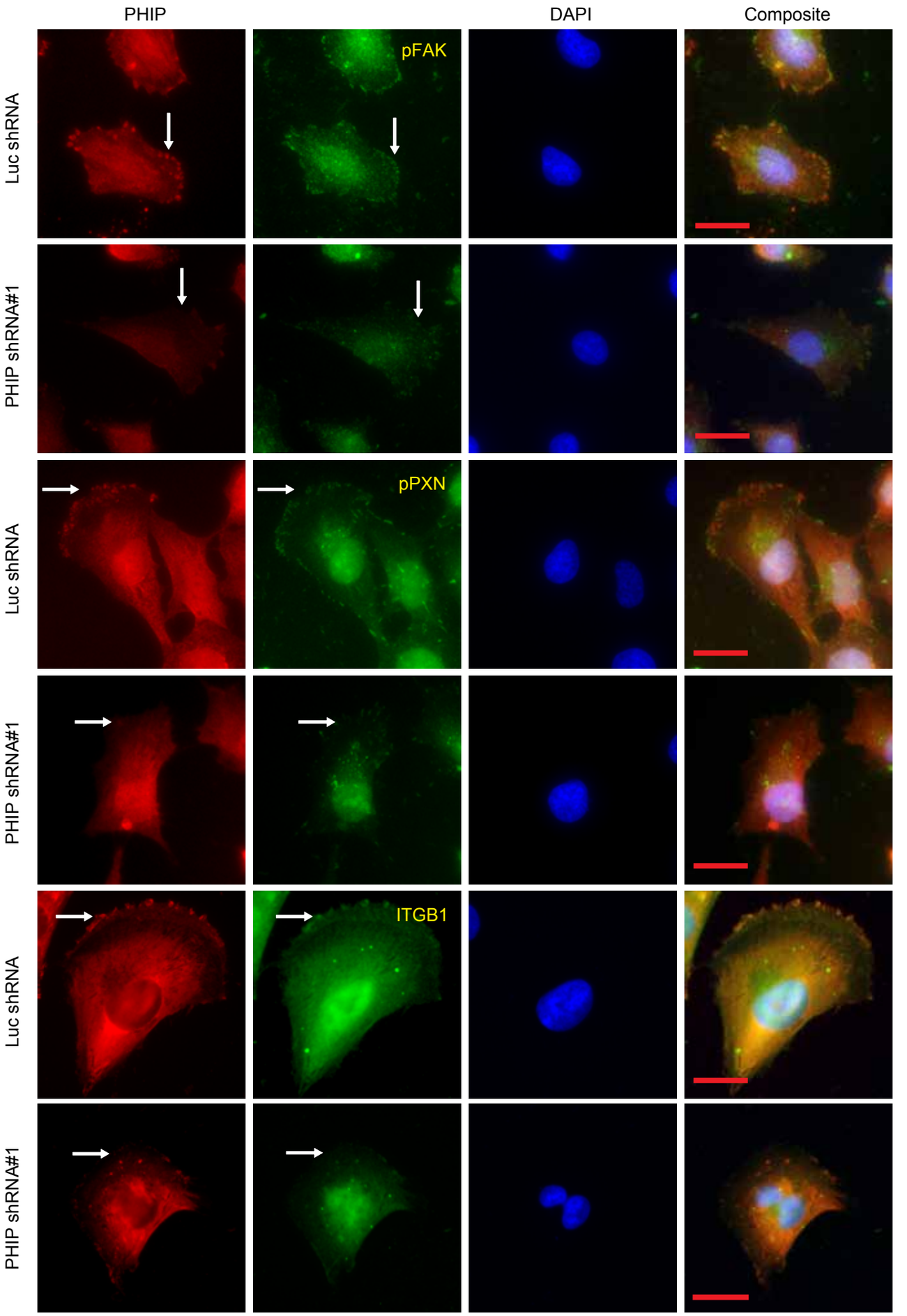
PHIP
DAPI
Composite
pFAK
pPXN
ITGB1
Luc shRNA
PHIP shRNA#1
Luc shRNA
PHIP shRNA#1
Luc shRNA
PHIP shRNA#1

Figure S5

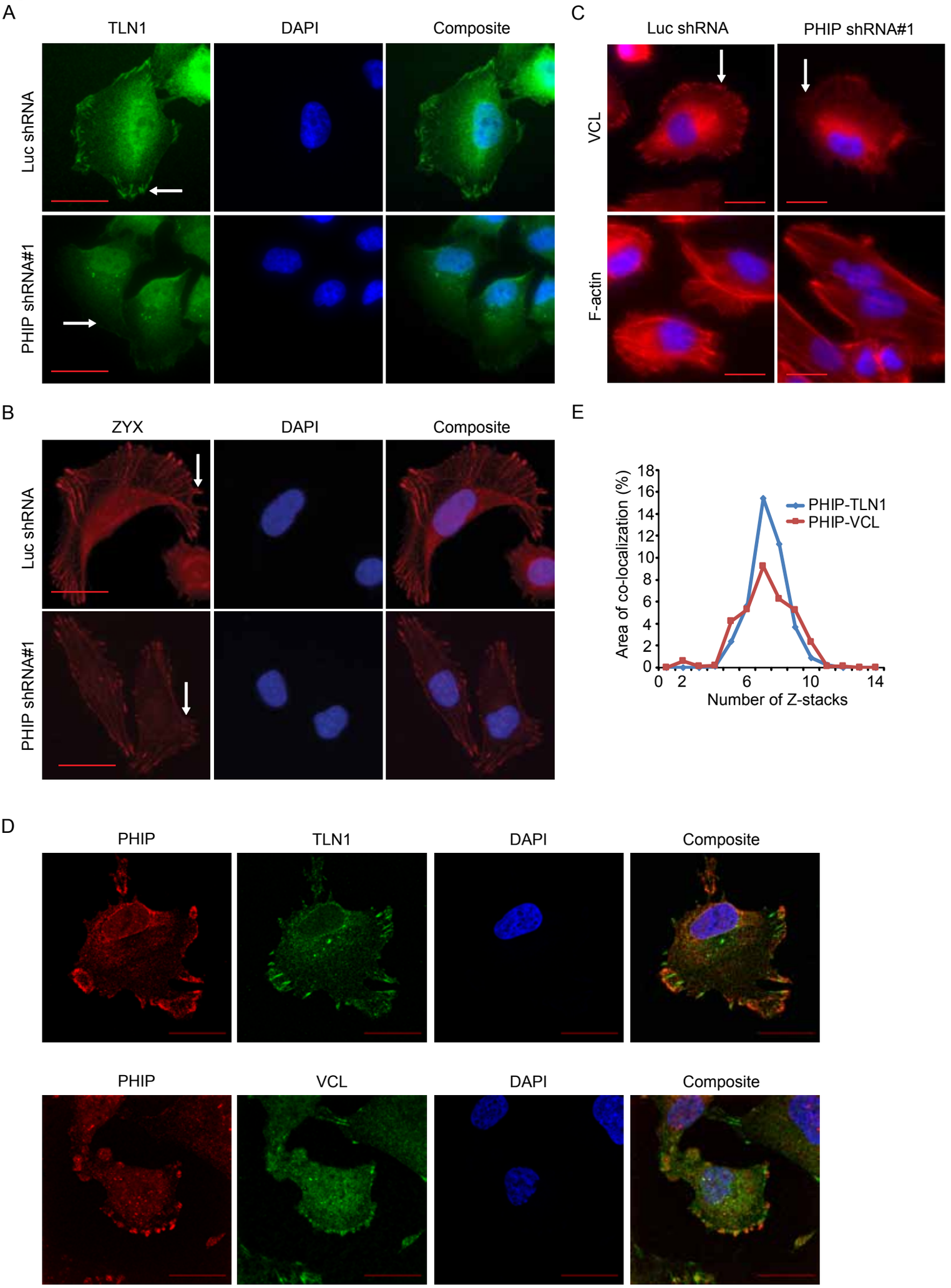
A
TLN1
DAPI
Composite
Luc shRNA
PHIP shRNA#1
C
Luc shRNA
PHIP shRNA#1
VCL
F-actin
B
ZYX
DAPI
Composite
Luc shRNA
PHIP shRNA#1
E
Area of co-localization (%)
PHIP-TLN1
PHIP-VCL
Number of Z-stacks
D
PHIP
TLN1
DAPI
Composite
PHIP
VCL
DAPI
Composite

Figure S6

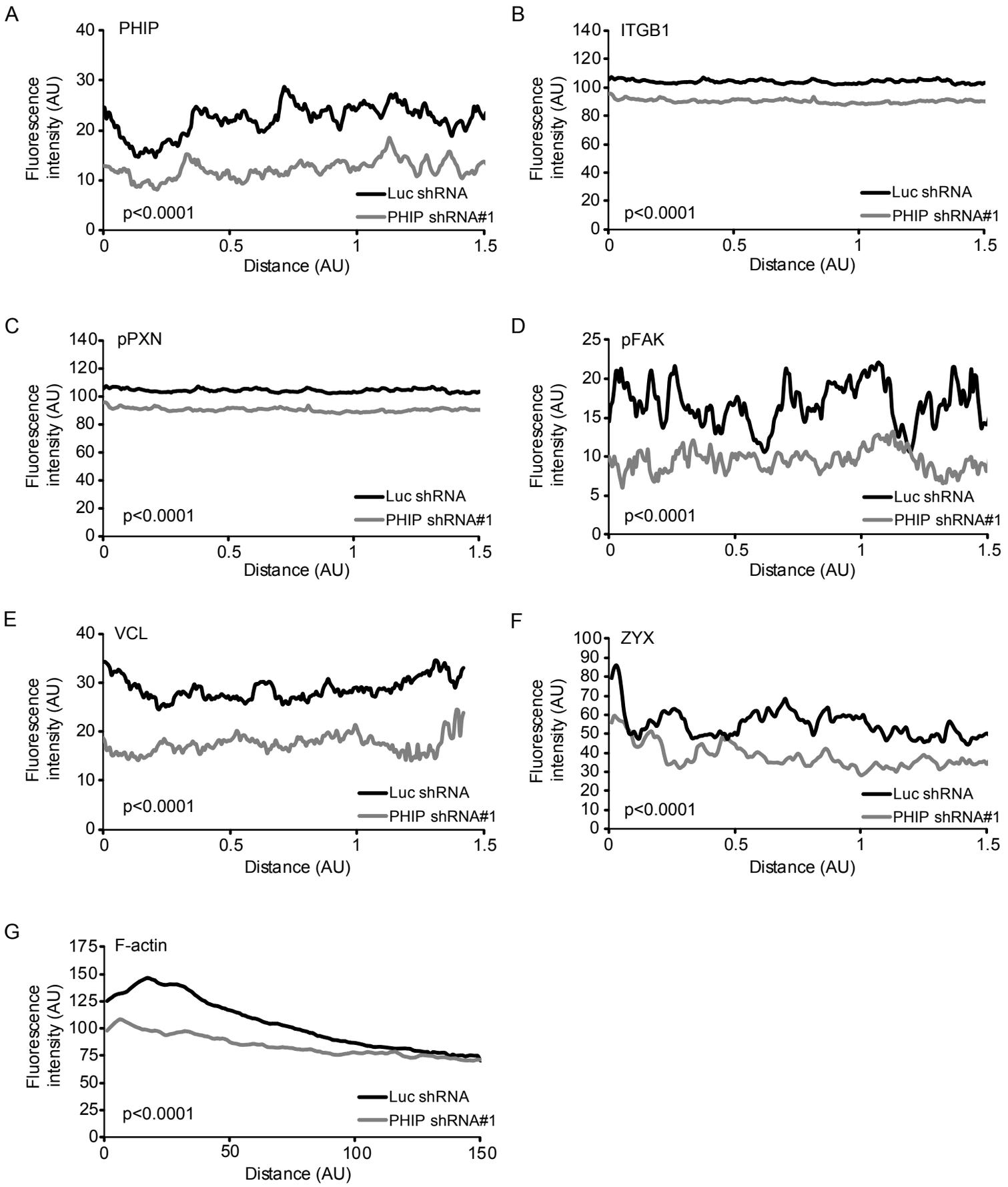
A
PHIP
Fluorescence intensity (AU)
Distance (AU)
Luc shRNA
PHIP shRNA#1
p<0.0001
B
ITGB1
C
pPXN
D
pFAK
E
VCL
F
ZYX
G
F-actin

Figure S7

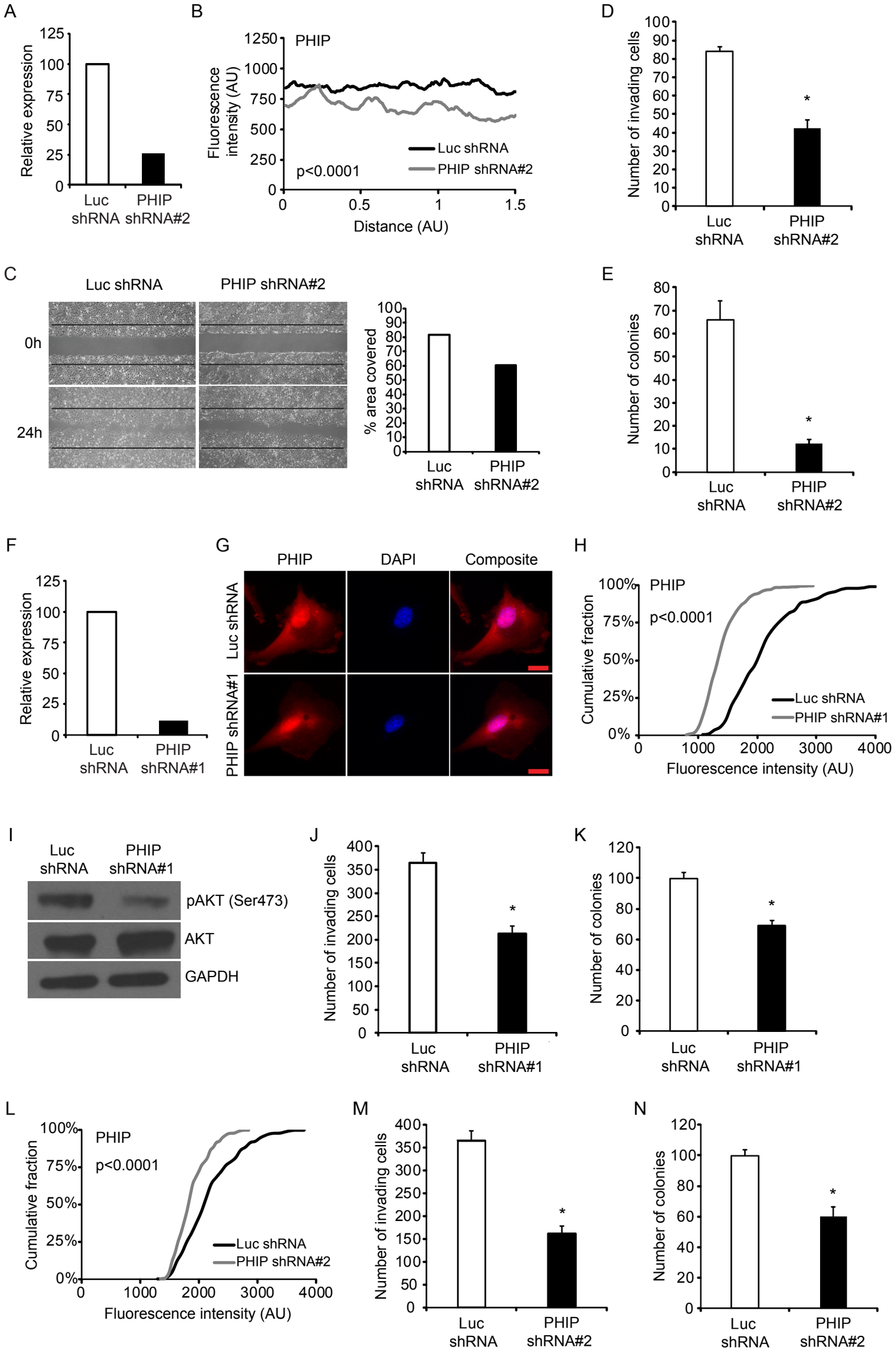
A
Relative expression
125
100
75
50
25
0
Luc shRNA
PHIP shRNA#2
B
PHIP
Fluorescence intensity (AU)
1250
1000
750
500
250
0
p<0.0001
Luc shRNA
PHIP shRNA#2
0
0.5
1
1.5
Distance (AU)
D
Number of invading cells
100
90
80
70
60
50
40
30
20
10
0
*
Luc shRNA
PHIP shRNA#2
C
Luc shRNA
PHIP shRNA#2
0h
24h
% area covered
100
90
80
70
60
50
40
30
20
10
0
Luc shRNA
PHIP shRNA#2
E
Number of colonies
80
70
60
50
40
30
20
10
0
*
Luc shRNA
PHIP shRNA#2
F
Relative expression
125
100
75
50
25
0
Luc shRNA
PHIP shRNA#1
G
PHIP
DAPI
Composite
Luc shRNA
PHIP shRNA#1
H
PHIP
p<0.0001
Cumulative fraction
100%
75%
50%
25%
0%
Luc shRNA
PHIP shRNA#1
0
1000
2000
3000
4000
Fluorescence intensity (AU)
I
Luc shRNA
PHIP shRNA#1
pAKT (Ser473)
AKT
GAPDH
J
Number of invading cells
400
350
300
250
200
150
100
50
0
*
Luc shRNA
PHIP shRNA#1
K
Number of colonies
120
100
80
60
40
20
0
*
Luc shRNA
PHIP shRNA#1
L
PHIP
p<0.0001
Cumulative fraction
100%
75%
50%
25%
0%
Luc shRNA
PHIP shRNA#2
0
1000
2000
3000
4000
Fluorescence intensity (AU)
M
Number of invading cells
400
350
300
250
200
150
100
50
0
*
Luc shRNA
PHIP shRNA#2
N
Number of colonies
120
100
80
60
40
20
0
*
Luc shRNA
PHIP shRNA#2

Figure S8

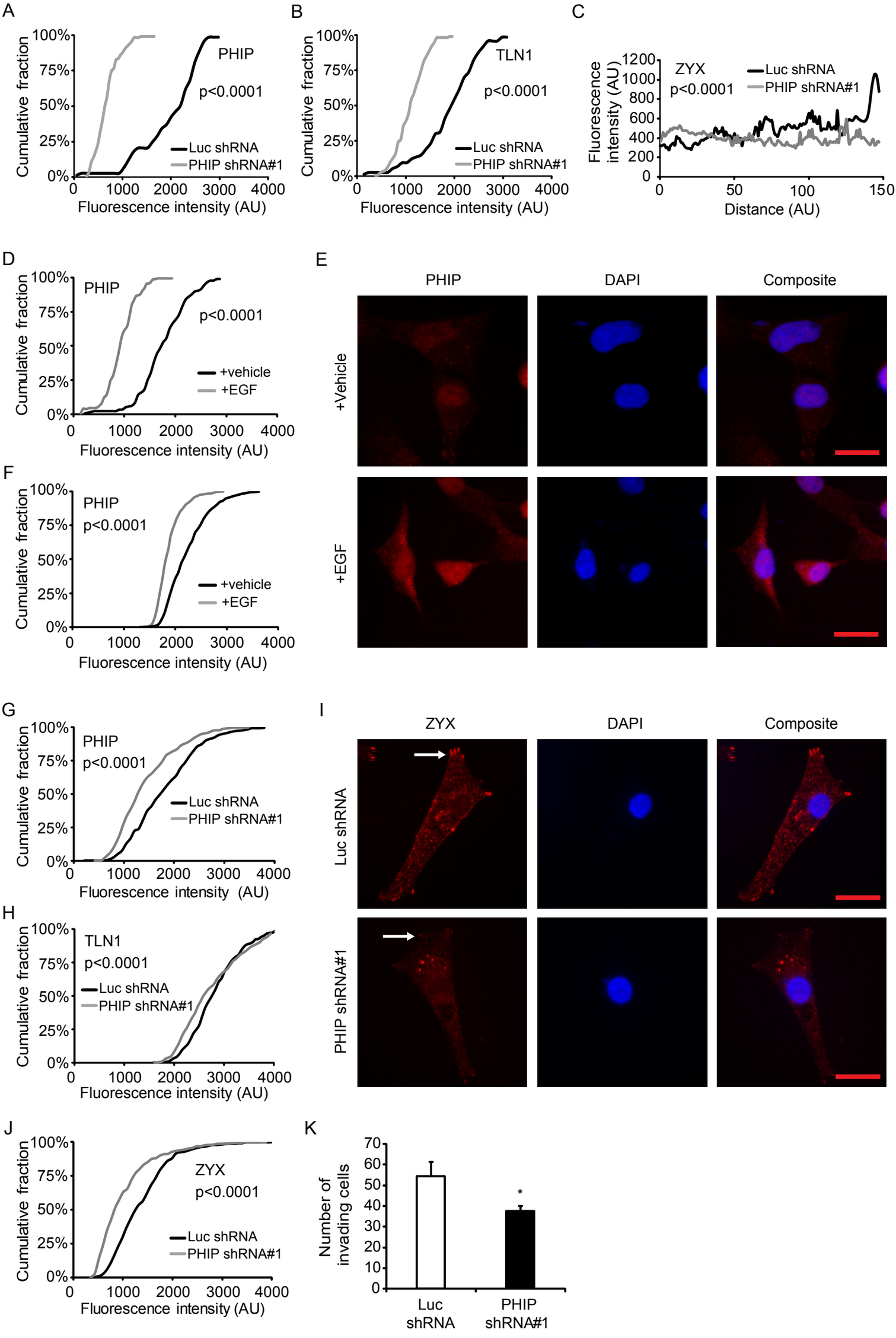
A
Cumulative fraction
100%
75%
50%
25%
0%
PHIP
p<0.0001
Luc shRNA
PHIP shRNA#1
0
1000
2000
3000
4000
Fluorescence intensity (AU)
B
TLN1
p<0.0001
C
ZYX
p<0.0001
Fluorescence intensity (AU)
1200
1000
800
600
400
200
0
50
100
150
Distance (AU)
D
+vehicle
+EGF
E
PHIP
DAPI
Composite
+Vehicle
+EGF
F
G
H
I
ZYX
Luc shRNA
PHIP shRNA#1
J
K
Number of invading cells
70
60
50
40
30
20
10
*
Luc shRNA
PHIP shRNA#1

Table S1: Molecular profiling and MGMT status of glioblastoma cases.

Case number	Diagnosis	MGMT status	Molecular subtyping*
180	Glioblastoma	Unmethylated	Clasical
188	Glioblastoma	Unmethylated	Classical
218	Glioblastoma	Unmethylated	Classical
179	Glioblastoma	Unmethylated	Classical
199	Glioblastoma	77.24%	Classical
170	Glioblastoma	Unmethylated	Classical
195	Glioblastoma	ND	Classical
192	Glioblastoma	Unmethylated	Classical
93	Glioblastoma	ND	Mesenchymal
160	Glioblastoma	Unmethylated	Mesenchymal
137	Glioblastoma	ND	Mesenchymal
182	Glioblastoma	Unmethylated	Mesenchymal
175	Glioblastoma	ND	Mesenchymal
224	Glioblastoma	Unmethylated	Mesenchymal
212	Glioblastoma	Unmethylated	Mesenchymal
47	Glioblastoma	ND	Mesenchymal
177	Glioblastoma	Unmethylated	Proneural
176	Glioblastoma	34.56%	Proneural
68	Glioblastoma	ND	Proneural
138	Glioblastoma	Unmethylated	Proneural
56	Glioblastoma	ND	Proneural
172	Glioblastoma	ND	Proneural
41	Oligodendroglioma	28.76%	Proneural
155	Glioblastoma	ND	Proneural
156	Glioblastoma	ND	Proneural

* Molecular subtyping by RNA Seq or Taqman.

ND: not determined